INTERNATIONAL JOURNAL FOR NUMERICAL METHODS IN FLUIDS
Int. J. Numer. Meth. Fluids 2008; **57**:693–713
Published online 15 November 2007 in Wiley InterScience (www.interscience.wiley.com). DOI: 10.1002/fld.1638

Modelling and numerical methods for the dynamics of impurities in a gas

E. Ferrari and L. Pareschi*, †

Department of Mathematics and Center for Modelling Computing and Statistics (*CMCS*), *University of Ferrara*, *Via Machiavelli 35*, *44100 Ferrara*, *Italy*

SUMMARY

The dynamics of a mixture of impurities in a gas can be represented by a system of linear Boltzmann equations for hard spheres. We assume that the background is in thermodynamic equilibrium and that the polluting particles are sufficiently few (in comparison with the background molecules) to admit that there are no collisions among couples of them. In order to derive non-trivial hydrodynamic models, we close the Euler system around local Maxwellian's which are not equilibrium states.

The kinetic model is solved by using a Monte Carlo method, the hydrodynamic one by implicit–explicit Runge–Kutta schemes with weighted essentially non-oscillatory reconstruction (*J. Sci. Comput.* 2005; **25**(1–2):129–155). Several numerical tests are then computed in order to compare the results obtained with the kinetic and the hydrodynamic models. Copyright © 2007 John Wiley & Sons, Ltd.

Received 23 November 2006; Revised 31 August 2007; Accepted 6 September 2007

KEY WORDS: inelastic collisions; Boltzmann equation; hydrodynamic models; Monte Carlo methods; IMEX Runge–Kutta schemes; WENO schemes

1. INTRODUCTION

In this paper, we consider the motion of a dilute gas of impurities in an equilibrium background gas. The background gas has a Maxwellian distribution with parameters determined by the Euler equations. The impurity distributions are determined from a set of Boltzmann equations with inelastic collisions. For a detailed discussion on the validity of the model we refer the reader to [1–4] and the references therein. For such a model we derive suitable Monte Carlo methods and consider the delicate problem of its approximation through a closed set of equations for the low-order moments.

From a physical viewpoint, the model is derived by considering the dynamics of a mixture of N species of impurities (treated as inelastic granular gases) constituted by particles with mass m_i

*Correspondence to: L. Pareschi, Department of Mathematics, University of Ferrara, Via Machiavelli 35, 44100 Ferrara, Italy.
†E-mail: lorenzo.pareschi@unife.it, pareschi@dm.unife.it

and diameter δ_i $(i=1,2,\ldots,N)$, which interact with a background gas constituted by molecules with mass m_b and diameter δ_b. If we assume the background gas in thermodynamic equilibrium and that particle impurities are sufficiently few to ignore collisions among couple of them, we obtain the set of N dissipative linear Boltzmann equations for hard spheres

$$\begin{aligned}\frac{\partial f_i}{\partial t}+\mathbf{v}\cdot\nabla_{\mathbf{x}} f_i &= \frac{1}{\varepsilon_{ib}}\frac{\delta_{ib}^2}{2\pi}\int_{\mathbb{R}^3\times S^2}|(\mathbf{v}-\mathbf{w})\cdot\mathbf{n}|\left[\frac{1}{e_{ib}^2}f_i(\mathbf{v}_*)M_b(\mathbf{w}_*)-f_i(\mathbf{v})M_b(\mathbf{w})\right]\mathrm{d}\mathbf{w}\,\mathrm{d}\mathbf{n}\\ M_b(\mathbf{v}) &= \left(\frac{1}{2\pi R_b T_b}\right)^{3/2}\exp\left\{-\frac{(\mathbf{v}-u_b)^2}{2R_bT_b}\right\}\end{aligned} \tag{1}$$

coupled with the Euler system

$$\begin{aligned}\frac{\partial \rho_b}{\partial t}+\nabla_{\mathbf{x}}\cdot(\rho_b u_b) &= 0\\ \frac{\partial \rho_b u_b}{\partial t}+\nabla_{\mathbf{x}}\cdot(\rho_b u_b\otimes u_b+\rho_b R_b T_b) &= 0\\ \frac{\partial E_b}{\partial t}+\nabla_{\mathbf{x}}\cdot(E_b u_b+\rho_b R_b T_b u_b) &= 0\end{aligned} \tag{2}$$

In the above equations, the subscript $i=1,\ldots,N$ refers to the impurity and the subscript b denotes the equilibrium background gas. The constant R_b is defined by $R_b=k_{\mathrm{B}}/m_b$, where k_{B} is the Boltzmann constant. Here ε_{ib} are the Knudsen numbers, $\delta_{ib}=(\delta_i-\delta_b)/2$ is the distance between the centers of the colliding particles and $\mathbf{n}\in\mathbb{S}^2$ is the unit vector of impact between the velocities $\mathbf{v}_*$ and $\mathbf{w}_*$ that collide returning $\mathbf{v}$ and $\mathbf{w}$.

The pre-collisional velocities are given implicitly by relations

$$\begin{aligned}\mathbf{v} &= \mathbf{v}_*-2\alpha_{bi}(1-\beta_{ib})[(\mathbf{v}_*-\mathbf{w}_*)\cdot\mathbf{n}]\mathbf{n}\\ \mathbf{w} &= \mathbf{w}_*+2(1-\alpha_{bi})(1-\beta_{ib})[(\mathbf{v}_*-\mathbf{w}_*)\cdot\mathbf{n}]\mathbf{n}\end{aligned} \tag{3}$$

with $\alpha_{ib}=m_i/(m_i+m_b)$, so that $\alpha_{bi}=1-\alpha_{ib}$ and $\beta_{ib}=(1-e_{ib})/2$, where $e_{ib}\in(0,1]$ is the coefficient of restitution between impurities and background molecules ($\beta_{ib}=0$ in the elastic case).

The linear collision operators conserve the particle number of each species of impurities and the total momentum, but part of the kinetic energy is dissipated according to the equation

$$(\mathbf{v}-\mathbf{w})\cdot\mathbf{n}=-e_{ij}(\mathbf{v}_*-\mathbf{w}_*)\cdot\mathbf{n} \tag{4}$$

For system (1) it is possible to prove (see [2, 3, 5]) that the stationary equilibrium states of the collision operators are given by the Maxwellian distributions

$$M_i^{\sharp}(\mathbf{v})=\left(\frac{1}{2\pi R_i T_i^{\sharp}}\right)^{3/2}\exp\left\{-\frac{(\mathbf{v}-u_b)^2}{2R_iT_i^{\sharp}}\right\},\quad \mathbf{v}\in\mathbb{R}^3 \tag{5}$$

having the same mean velocity of the background and temperatures

$$T_i^{\sharp}=\frac{(1-\alpha_{bi})(1-\beta_{ib})}{1-\alpha_{bi}(1-\beta_{ib})}T_b \tag{6}$$

lower than the background one. Here $R_i=k_{\mathrm{B}}/m_i$.

DOI: 10.1002/fld

Although the methods we will describe in the sequel apply straightforwardly to the general case of systems of impurities, for simplicity we will reduce to the case of a single type of impurity ($N=1$), so that problem (1) is reduced to

$$\frac{\partial f}{\partial t}+\mathbf{v}\cdot\nabla_{\mathbf{x}} f=\frac{\delta^2}{2\pi\varepsilon}\int_{\mathbb{R}^3\times S^2}|(\mathbf{v}-\mathbf{w})\cdot\mathbf{n}|\left[\frac{1}{e^2}f(\mathbf{v}_*)M_b(\mathbf{w}_*)-f(\mathbf{v})M_b(\mathbf{w})\right]\mathrm{d}\mathbf{w}\,\mathrm{d}\mathbf{n} \tag{7}$$

where $f=f_1$ is the distribution function of the impurities, $\delta=\delta_{1b}$ is the distance between the centers of the colliding particles, $e=e_{1b}$ is the restitution coefficient in the mixed collision, $\varepsilon=\varepsilon_{1b}$ is the Knudsen number and $R=k_{\mathrm{B}}/m$ is a constant depending on the mass $m=m_1$ of the particles. We will also denote with $\alpha=\alpha_{bi}$ and $\beta=\beta_{ib}$.

We remark that in this paper the interaction of the impurities with the background gas occurs through binary collisions. If the size of the impurities is significantly larger than that of molecules of the background, a Fokker–Planck description may be more appropriate. For example, in the limit $\alpha\to 0$ a Fokker–Planck equation has been derived in [6]. A different approach has been used in [2] to study the relationship between a Boltzmann and a Fokker–Planck description of the system. However, a detailed comparison of the validity of these different models goes beyond the scope of the present paper.

The remainder of this paper is organized as follows: Section 2 is devoted to the problem of the derivation of suitable hydrodynamic models for the system of impurities. Next, we introduce the Monte Carlo method applied to the kinetic model in our simulations. Then, we describe the implicit–explicit (IMEX) Runge–Kutta schemes used to solve the hydrodynamic models numerically. Finally, we present some numerical tests and compare the results obtained with the two models and the corresponding numerical methods.

2. HYDRODYNAMIC MODELS

In this section, we summarize the derivation of hydrodynamic models from the kinetic one. We first consider the so-called *pseudo-Maxwellian case*, then the *hard spheres case* (see [3, 7, 8]). The pseudo-Maxwellian approximation consists in replacing the relative velocity $\mathbf{q}$ by a different vector $S(\mathbf{x},t)\bar{\mathbf{q}}$, where S is independent of the integration variables and $\bar{\mathbf{q}}=\mathbf{q}/|\mathbf{q}|$. For simplicity, we assume that without loss of generality $S(x,t)=1$.

In both cases considered, the existence of a Maxwellian equilibrium at non-zero temperature (5) allows one to construct hydrodynamic models for the granular flow. However, here only the mass of the inelastic particles is preserved. Thus, the mass ρ is the unique hydrodynamic variable and the Euler system is reduced to the single advection equation

$$\frac{\partial\rho}{\partial t}+\nabla_{\mathbf{x}}\cdot(\rho u)=0 \tag{8}$$

To obtain more detailed hydrodynamic models, one can rely on different entropy functionals [9]. Here, we consider a logarithmic entropy functional [7, 9] that corresponds to perform a closure for the moment equations by replacing f with the local Maxwellian

$$M(\rho,u,T)=\left(\frac{1}{2\pi RT}\right)^{3/2}\exp\left\{-\frac{(\mathbf{v}-u)^2}{2RT}\right\},\quad \mathbf{v}\in\mathbb{R}^3$$

DOI: 10.1002/fld

where ρ, u and T are the density, mean velocity and temperature of f at time t given by

$$\begin{aligned}\rho &= \int_{\mathbb{R}^3} f(\mathbf{v},t)\,\mathrm{d}\mathbf{v}\\ u &= \frac{1}{\rho}\int_{\mathbb{R}^3} \mathbf{v} f(\mathbf{v},t)\,\mathrm{d}\mathbf{v}\\ T &= \frac{1}{3R\rho}\int_{\mathbb{R}^3} (\mathbf{v}-u)^2 f(\mathbf{v},t)\,\mathrm{d}\mathbf{v}\end{aligned} \tag{9}$$

Of course, the validity of this assumption may be questionable and one of the aims of the present paper is in fact to verify numerically the results obtained under this closure.

In order to avoid the term $1/e^2$ in the right-hand side of (7) and obtain the equations for the moments, it is useful to consider the weak form of the Boltzmann equation.

Given any test-function $\varphi(\mathbf{v})$, we have

$$\langle \varphi, Q(f, M_b)\rangle = \frac{\delta^2}{2\pi\varepsilon}\int_{\mathbb{R}^3_{\mathbf{w}}\times\mathbb{R}^3_{\mathbf{v}}\times S^2} |\mathbf{q}\cdot\mathbf{n}|(\varphi(\mathbf{v}^*)-\varphi(\mathbf{v}))f(\mathbf{v})M_b(\mathbf{w})\,\mathrm{d}\mathbf{w}\,\mathrm{d}\mathbf{v}\,\mathrm{d}\mathbf{n} \tag{10}$$

where $\langle\cdot,\cdot\rangle$ represents the inner product in $L^1(\mathbb{R}^3)$ and the post-collisional velocity $\mathbf{v}^*$ is defined as

$$\mathbf{v}^* = \mathbf{v} - 2\alpha(1-\beta)(\mathbf{q}\cdot\mathbf{n})\mathbf{n} \tag{11}$$

As usual, we choose as test functions, respectively, $\varphi = 1$ (which is the unique collision invariant), $\varphi = \mathbf{v}$ and $\varphi = \frac{1}{2}|\mathbf{v}|^2$.

As shown in [3, 7], the weak form of the Boltzmann equation for pseudo-Maxwellian molecules leads to the following dissipative Euler system:

$$\begin{aligned}\frac{\partial\rho}{\partial t} + \nabla_{\mathbf{x}}\cdot(\rho u) &= 0\\ \frac{\partial\rho u}{\partial t} + \nabla_{\mathbf{x}}\cdot(\rho u\otimes u + \rho RT) &= -\frac{\alpha(1-\beta)}{\varepsilon}\rho\rho_b(u-u_b)\\ \frac{\partial}{\partial t}\left(\rho\left(\frac{1}{2}|u|^2+\frac{3}{2}RT\right)\right) + \nabla_{\mathbf{x}}\cdot\left(\rho u\left(\frac{1}{2}|u|^2+\frac{5}{2}RT\right)\right) &= \frac{\rho\rho_b}{\varepsilon}D(\mathbf{x},t)\end{aligned} \tag{12}$$

with

$$D(\mathbf{x},t) = \alpha(1-\beta)(u-u_b)^2 - u(u-u_b) - 3R[1-\alpha(1-\beta)](T-T^{\natural})$$

The quantity $\rho(\frac{1}{2}|u|^2+\frac{3}{2}RT)$ represents the energy $E = \frac{1}{2}\int_{\mathbb{R}^3}|\mathbf{v}|^2 f(\mathbf{v},t)\,\mathrm{d}\mathbf{v}$ under the assumption of a monoatomic granular gas.

DOI: 10.1002/fld

If we apply the same procedure to the hard spheres case, we obtain

$$\frac{\partial \rho}{\partial t}+\nabla_{\mathbf{x}}\cdot(\rho u)=0$$

$$\frac{\partial \rho u}{\partial t}+\nabla_{\mathbf{x}}\cdot(\rho u\otimes u+\rho RT)=-\frac{\alpha(1-\beta)}{\varepsilon}\rho\rho_b\sqrt{\frac{2\psi(T)}{\pi R}}A(x,t) \tag{13}$$

$$\frac{\partial}{\partial t}\left(\rho\left(\frac{1}{2}|u|^2+\frac{3}{2}RT\right)\right)+\nabla_{\mathbf{x}}\cdot\left(\rho u\left(\frac{1}{2}|u|^2+\frac{5}{2}RT\right)\right)=\frac{\alpha(1-\beta)}{\varepsilon}\rho\rho_b\sqrt{\frac{2\psi(T)}{\pi R}}B(x,t)$$

where

$$A(x,t)=\frac{4}{3}\left[\frac{2R}{\psi(T)}+\frac{(u-u_b)^2}{5}\right](u-u_b)$$

$$B(x,t)=\frac{(u-u_b)^4}{5}\left[\alpha(1-\beta)+\frac{\psi(T)T}{3}\right]+\frac{4R}{\psi(T)}(u-u_b)^2\left[\alpha(1-\beta)-\frac{\psi(T)T}{3}\right]$$

$$-\frac{4}{15}u(u-u_b)^3-\frac{8R}{3\psi(T)}u(u-u_b)+\frac{8R^2}{\psi(T)^2}[\alpha(1-\beta)-\psi(T)T]$$

and

$$\psi(T)=\frac{\alpha}{(1-\alpha)T_b+\alpha T}$$

Remark 1
It should be noted that both the limiting models are described by conservation laws with sources. The classical case of elastic collisions can be recovered taking $\beta=0$ and hence $T^{\sharp}=T^b$. The major difference between Maxwell and hard spheres is the nonlinear dependence from the temperature in the relaxation terms for the mean velocity and the temperature itself.

3. HYBRID MONTE CARLO METHODS FOR THE KINETIC MODEL

In order to solve the kinetic system numerically, we consider the development of a hybrid scheme in which we simulate the evolution of the particles according to the following methods [10]:

- The background moments ρ_b, u_b, T_b are computed using a deterministic method (finite volume/finite differences/finite elements).
- The particle evolution is computed with a probabilistic method (direct simulation Monte Carlo).

The two steps are connected by sampling the background velocities from the Maxwellian distribution $M_b=M(\rho_b,u_b,T_b)$. This can be done in a conservative way as in [11–13].

DOI: 10.1002/fld

During the interaction, the velocity of a particle of impurity changes following the relation

$$\mathbf{v}' = \mathbf{v} - 2\alpha(1-\beta)[(\mathbf{v}-\mathbf{w})\cdot\mathbf{n}]\mathbf{n} \tag{14}$$

where $\alpha = \alpha_{b1}$ and $\beta = \beta_{1b}$.

Using the identity

$$\int_{S_2} (\mathbf{q}\cdot\mathbf{n})_+ \phi((\mathbf{q}\cdot\mathbf{n})\mathbf{n})\,\mathrm{d}\mathbf{n} = \frac{|\mathbf{q}|}{4}\int_{S_2} \phi\left(\frac{\mathbf{q}-|\mathbf{q}|\mathbf{n}}{2}\right)\mathrm{d}\mathbf{n}$$

we can rewrite (14) as

$$\mathbf{v}' = \mathbf{v} - \alpha(1-\beta)[(\mathbf{v}-\mathbf{w}) - |\mathbf{v}-\mathbf{w}|\mathbf{n}] \tag{15}$$

The unit vector $\mathbf{n}$ is chosen uniformly in the unit sphere; hence, it is

$$\mathbf{n} = \begin{pmatrix} \cos\phi\sin\theta \\ \sin\phi\sin\theta \\ \cos\theta \end{pmatrix} \tag{16}$$

where $\theta = \arccos(2\xi_1 - 1)$ and $\phi = 2\pi\xi_2$, with ξ_1, ξ_2 being uniformly distributed random variables in $[0, 1]$.

The starting point of the DSMC methods is the usual first-order splitting in time of the Boltzmann equation (7), which consists in solving separately a purely convective step and a collision step characterized by a space homogeneous Boltzmann equation (i.e. $\nabla_{\mathbf{x}} f \equiv 0$). Clearly, after this splitting, almost all the main difficulties are contained in the collision step, so that we fix our attention on the homogeneous Boltzmann equation

$$\frac{\partial f}{\partial t} = \frac{1}{\varepsilon} Q(f, M_b) \tag{17}$$

It is equivalent to a differential system of the type

$$\frac{\partial f}{\partial t} = \frac{1}{\varepsilon}[P(f, M_b) - \mu f] \tag{18}$$

where $\mu \neq 0$ is a constant and P a bilinear operator.

In the space homogeneous case, the operator $P(f, M_b)$ for variable hard spheres is given by

$$P(f, M_b) = Q^+(f, M_b) + f(\mathbf{v})\left(\mu - 4\pi\int_{\mathbb{R}^3} |\mathbf{v}-\mathbf{w}| M_b(\mathbf{w})\,\mathrm{d}\mathbf{w}\right) \tag{19}$$

The operator $Q^+(f, M_b)$ is the gain term of the collision operator $Q(f, M_b)$, so that the constant μ is a bound on the loss term and has to satisfy the relation

$$\mu \geqslant 4\pi\int_{\mathbb{R}^3} |\mathbf{v}-\mathbf{w}| M_b(\mathbf{w})\,\mathrm{d}\mathbf{w} \tag{20}$$

Since we deal with a finite set of particles, there is no restriction in practice by replacing the kernel $|\mathbf{v}-\mathbf{w}|$ with the bounded kernel

$$|\mathbf{v}-\mathbf{w}|_\Sigma = \min(|\mathbf{v}-\mathbf{w}|, \Sigma), \quad \Sigma > 0$$

DOI: 10.1002/fld

In this case, in order to satisfy (20), it is enough to choose

$$\mu = 4\pi\Sigma\rho_b$$

where ρ_b is the background mass.

The classical DSMC fictitious collision method for variable hard spheres with acceptance–rejection strategy is then applied, so that the collision between a particle of impurity, having velocity v_i, and one of background, with velocity w_j, occurs only if

$$\Sigma\xi < |v_i - w_j|$$

where $\xi \in [0, 1]$ is a uniformly distributed random variable and the upper bound Σ should be given by

$$\Sigma = \max_{i,j} |v_i - w_j|$$

The conservative DSMC algorithm for VHS collision kernels, adapted to the mixture interaction, can be expressed as follows.

Algorithm 1. Nambu–Babovsky for VHS molecules

---

1. *compute the initial velocity of the particles*, $\{v_i^0, i = 1, \ldots, N\}$,
   by sampling them from the initial density $f_0(v)$
2. *compute the velocity of N background molecules* $\{w_j^0, j = 1, \ldots, N\}$,
   by sampling them from the Maxwellian distribution $M_b(w)$
3. `for` $n = 1, \ldots, n_{TOT}$
   given $\{v_i^n, i = 1, \ldots, N\}$
   - *compute an upper bound* Σ *of the cross section*
   - *set* $N_c = Iround(N\rho_b\Sigma\Delta t/\varepsilon)$
   - *select* N_c *dummy collision pairs* (i, j) *uniformly among all possible pairs, and for those*
     - *compute the relative cross section* $B_{ij} = B(|v_i - w_j|)$
     - `if` $\Sigma\xi < B_{ij}$
       - *perform the collision between* i *and* j *and compute* v_i' *according to the collisional law*
       - *set* $v_i^{n+1} = v_i'$
   - *set* $v_i^{n+1} = v_i^n$ *for all the particles that have not collided*

   `end for`

The expected number of particles that collide with a background one (i.e. the number of collisions) in a small time step Δt is $N\rho_b\Sigma\Delta t/\varepsilon$. $Iround(x)$ denotes a suitable integer rounding of a positive real number x.

DOI: 10.1002/fld

The computation of the upper bound Σ, if N is the number of colliding couples, requires $O(N^2)$ operations. However, taking the larger bound

$$\Sigma = \max_i |v_i - \bar{u}| + \max_j |w_j - \bar{u_b}| + |\bar{u} - \bar{u_b}|$$

we can reduce the computational cost at $O(N)$. Here, we denote the mean velocities, respectively, of the background and the impurities by $\bar{u_b}$ and $\bar{u}$.

We refer to [14] and references therein for further details on the DSMC method for the Boltzmann equation.

4. IMEX-WENO SCHEMES FOR THE FLUID MODEL

To solve numerically the hydrodynamic models (12) and (13) we apply the *IMEX Runge–Kutta schemes* up to the third order [15]. These schemes are strong-stability-preserving (SSP) for the limiting system of conservation laws in the limit of vanishing Knudsen number. These schemes assure the asymptotic preserving property, i.e. the consistency of the scheme with the equilibrium system and the asymptotic accuracy, so that the order of accuracy is also maintained in the zero relaxation limit. The high accuracy in space is obtained by using a *weighted essentially non-oscillatory* (*WENO*) *reconstruction* [16].

Let us summarize shortly the construction of such schemes.

4.1. IMEX Runge–Kutta schemes

In one-space dimension, a hyperbolic system with relaxation for conservative variables has the form

$$\partial_t U + \partial_x F(U) = \frac{1}{\varepsilon} R(U), \quad x \in \mathbb{R} \tag{21}$$

The Jacobian matrix $F'(U)$ has real eigenvalues and admits a basis of eigenvectors $\forall U \in \mathbb{R}^n$. ε is the *relaxation parameter*.

An IMEX Runge–Kutta scheme consists in applying an implicit discretization to the source terms and an explicit one to the non-stiff term. When applied to the previous system, it takes the form

$$\begin{aligned} U^{(i)} &= U^n - \Delta t \sum_{j=1}^{i-1} \tilde{a}_{ij} \partial_x F(U^{(j)}) + \Delta t \sum_{j=1}^{v} a_{ij} \frac{1}{\varepsilon} R(U^{(j)}) \\ U^{n+1} &= U^n - \Delta t \sum_{i=1}^{v} \tilde{w}_i \partial_x F(U^{(i)}) + \Delta t \sum_{i=1}^{v} w_i \frac{1}{\varepsilon} R(U^{(i)}) \end{aligned} \tag{22}$$

The matrices $\tilde{A} = (\tilde{a}_{ij})$, $\tilde{a}_{ij} = 0$ for $j \geqslant i$ and $A = (a_{ij})$ are $v \times v$ matrices such that the resulting scheme is explicit in F and implicit in R. An IMEX Runge–Kutta scheme is characterized by these two matrices and the coefficient vectors $\tilde{w} = (\tilde{w}_1, \ldots, \tilde{w}_v)^{\mathrm{T}}$ and $w = (w_1, \ldots, w_v)^{\mathrm{T}}$.

Since the simplicity and efficiency of solving the algebraic equations corresponding to the implicit part of the discretization at each step are of paramount importance, it is natural to consider *diagonally implicit Runge–Kutta* (DIRK) *schemes* for the source terms ($a_{ij} = 0$, for $j > i$).

DOI: 10.1002/fld

Table I. Tableau for the explicit (left) and implicit (right) IMEX-SSP2(2, 2, 2) L-stable scheme.

0	0	0	γ	γ	0	$\gamma = 1 - \frac{1}{\sqrt{2}}$
1	1	0	$1-\gamma$	$1-2\gamma$	γ	
	1/2	1/2		1/2	1/2	

Table II. Tableau for the explicit (left) and implicit (right) IMEX-SSP3(4, 3, 3) L-stable scheme.

0	0	0	0	0	α	α	0	0	0
0	0	0	0	0	0	$-\alpha$	α	0	0
1	0	1	0	0	1	0	$1-\alpha$	α	0
1/2	0	1/4	1/4	0	1/2	β	η	$1/2-\beta-\eta-\alpha$	α
	0	1/6	1/6	2/3		0	1/6	1/6	2/3

$\alpha = 0.24169426078821, \quad \beta = 0.06042356519705 \quad \eta = 0.12915286960590$

IMEX Runge–Kutta schemes can be represented by a double *tableau* in the usual Butcher notation,

$$\begin{array}{c|c} \tilde{c} & \tilde{A} \\ \hline & \tilde{w}^{\mathrm{T}} \end{array} \qquad \begin{array}{c|c} c & A \\ \hline & w^{\mathrm{T}} \end{array}$$

where the coefficients $\tilde{c}$ and c used for the treatment of non-autonomous systems are given by the usual relation

$$\tilde{c}_i = \sum_{j=1}^{i-1} \tilde{a}_{ij}, \quad c_i = \sum_{j=1}^{i} a_{ij} \tag{23}$$

The use of a DIRK scheme for R is a sufficient condition to guarantee that F is always evaluated explicitly.

In all the schemes we have considered that the implicit *tableau* corresponds to an L-stable scheme, that is, $w^{\mathrm{T}} A^{-1} e = 1$, e being a vector whose components are all equal to 1, whereas the explicit tableau is SSPk, where k denotes the order of the SSP scheme. We shall use the notation SSP$k(s, \sigma, p)$, where the triplet (s, σ, p) characterizes the number s of stages of the implicit scheme, the number σ of stages of the explicit scheme and the order p of the IMEX scheme.

In particular, we will make use of the asymptotically SSP schemes of second and third order reported in Tables I and II.

DOI: 10.1002/fld

4.2. Finite difference IMEX-WENO schemes

For simplicity, we consider the case of the single scalar equation

$$u_t + f(u)_x = \frac{1}{\varepsilon} r(u) \tag{24}$$

It is necessary to distinguish between schemes based on cell averages (finite volume approach, widely used for conservation laws) and schemes based on point values (finite difference approach). In this work we apply the second approach, useful even if the implicit step cannot be explicitly solved.

Let Δx and Δt be the mesh widths. We introduce the grid points

$$x_j = j\Delta x, \quad x_{j+1/2} = x_j + \tfrac{1}{2}\Delta x, \quad j = \ldots, -2, -1, 0, 1, 2, \ldots$$

and use the standard notations

$$u_j^n = u(x_j, t^n), \quad \bar{u}_j^n = \frac{1}{\Delta x} \int_{x_{j-1/2}}^{x_{j+1/2}} u(x, t^n)\, \mathrm{d}x$$

In a finite difference scheme, the basic unknown is the pointwise value of the function, rather than its cell average. Osher and Shu observed that it is possible to write a finite difference scheme in conservative form [17]. Let us consider Equation (24) and express

$$\frac{\partial f}{\partial x}(u(x,t)) = \frac{\hat{f}\left(u\left(x + \dfrac{\Delta x}{2}, t\right)\right) - \hat{f}\left(u\left(x - \dfrac{\Delta x}{2}, t\right)\right)}{\Delta x}$$

The relationship between f and $\hat{f}$ is as follows. Let us consider the sliding average operator

$$\bar{u}(x,t) = \langle u \rangle_x \equiv \frac{1}{\Delta x} \int_{x-\Delta x/2}^{x+\Delta x/2} u(\xi, t)\, \mathrm{d}\xi$$

Differentiating with respect to x one obtains

$$\frac{\partial \bar{u}}{\partial x} = \frac{1}{\Delta x}\left(u\left(x + \frac{\Delta x}{2}, t\right) - u\left(x - \frac{\Delta x}{2}, t\right)\right)$$

Therefore, the relationship between f and $\hat{f}$ is the same as that exists between $\bar{u}(x,t)$ and $u(x,t)$, namely, flux function f is the cell average of the function $\hat{f}$. This also suggests a way to compute the flux function. The technique that is used to compute pointwise values of $u(x,t)$ at the edge of the cell from cell averages of u can be used to compute $\hat{f}(u(x_{j+1/2}, t))$ from $f(u(x_j, t))$. This means that in the finite difference method it is the flux function that is computed at x_j and then reconstructed at $x_{j+1/2}$. But the reconstruction at $x_{j+1/2}$ may be discontinuous. Which value should one use? A general answer to this question can be given if one considers flux functions that can be split

$$f(u) = f^+(u) + f^-(u) \tag{25}$$

with the condition that

$$\frac{\mathrm{d}f^+(u)}{\mathrm{d}u} \geqslant 0, \quad \frac{\mathrm{d}f^-(u)}{\mathrm{d}u} \leqslant 0 \tag{26}$$

DOI: 10.1002/fld

There is a close analogy between flux splitting and numerical flux functions. In fact, if a flux can be split as (25), then

$$F(a,b)=f^{+}(a)+f^{-}(b)$$

will define a monotone consistent flux, provided condition (26) is satisfied. Together with non-oscillatory reconstructions (such as WENO) and SSP time discretization, the monotonicity condition will ensure that the overall scheme will not produce spurious numerical oscillations [15]. This is the case of the local Lax–Friedrichs flux with conservative variables used in this paper.

A finite difference scheme therefore takes the following form:

$$\frac{\mathrm{d}u_j}{\mathrm{d}t}=-\frac{1}{\Delta x}[\hat{F}_{j+1/2}-\hat{F}_{j-1/2}]+\frac{1}{\varepsilon}g(u_j)$$

$$\hat{F}_{j+1/2}=\hat{f}^{+}(u^{-}_{j+1/2})+\hat{f}^{-}(u^{+}_{j+1/2})$$

$\hat{f}^{+}(u^{-}_{j+1/2})$ is obtained by

- computing $f^{+}(u_l)$ and interpreting it as cell average of $\hat{f}^{+}$;
- performing pointwise reconstruction of $\hat{f}^{+}$ in cell j and evaluating it in $x_{j+1/2}$.

$\hat{f}^{-}(u^{+}_{j+1/2})$ is obtained by

- computing $f^{-}(u_l)$ and interpreting it as cell average of $\hat{f}^{-}$;
- performing pointwise reconstruction of $\hat{f}^{-}$ in cell $j+1$ and evaluating it in $x_{j+1/2}$.

The treatment presented for the scalar equation can be extended to systems, with a minor change in notation. A detailed account on high-order finite difference schemes can be found in [16].

Remark 1

Let us finally remark that because of the non-linearity of the terms $A(x,t)$ and $B(x,t)$ in (13), the corresponding implicit solver has been solved by using a Newton's method.

5. NUMERICAL TESTS

We are interested in comparing the results obtained with the kinetic model and the hydrodynamic model (13) in the case of hard spheres.

The tests presented in this section differ for the initial condition of the impurities, whereas the background for simplicity is assumed to be constant, with mass, mean velocity and temperature given by

$$\rho_b=u_b=T_b=1$$

All the results refer to $\alpha=0.01$ and $\beta=0.1$. In all the graphics presented in this section, we plot the initial condition for the DSMC together with the solution obtained by DSMC and the solution with IMEX-SSP2$(2,2,2)$ and/or IMEX-SSP3$(4,3,3)$.

DOI: 10.1002/fld

5.1. Inert concentration of impurities

In the first test case we consider a concentration of impurities, transported by a constant wind in 1-D. The evolution is studied for different values of the Knudsen number, namely

$$\varepsilon = 0.1, 0.005, 0.0001$$

The mass density of the impurities consists in a square wave profile characterized by $\rho = 1$ for $0.2 \leqslant x \leqslant 0.4$ and $\rho = 0$ elsewhere. The mean velocity is assumed to be zero ($u = 0$) and the temperature to be small ($T = 0.05$). The boundary conditions are periodic.

As shown in Figures 1–6, there is good agreement between the results obtained with the different models for all ranges of Knudsen numbers.

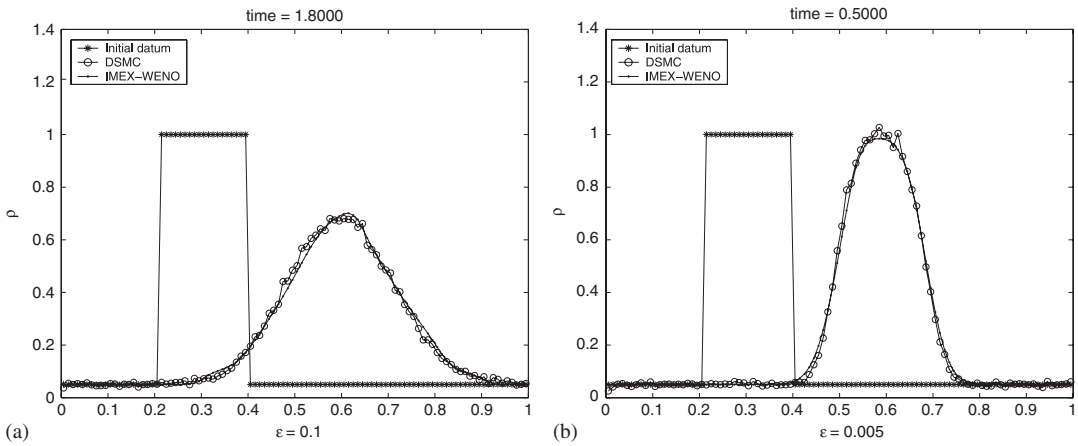

Figure 1. Test 1—evolution of the mass density with $\varepsilon = 0.1$ (a) and $\varepsilon = 0.005$ (b).

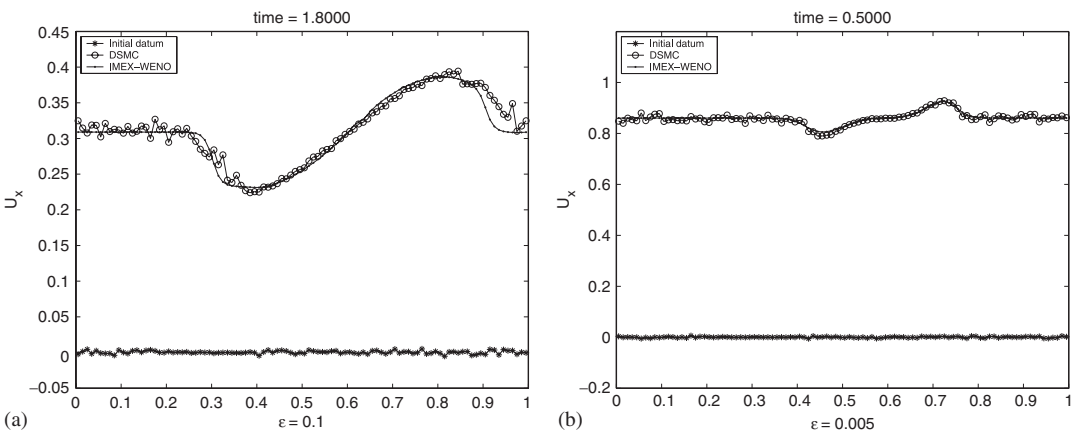

Figure 2. Test 1—evolution of the velocity with $\varepsilon = 0.1$ (a) and $\varepsilon = 0.005$ (b).

DOI: 10.1002/fld

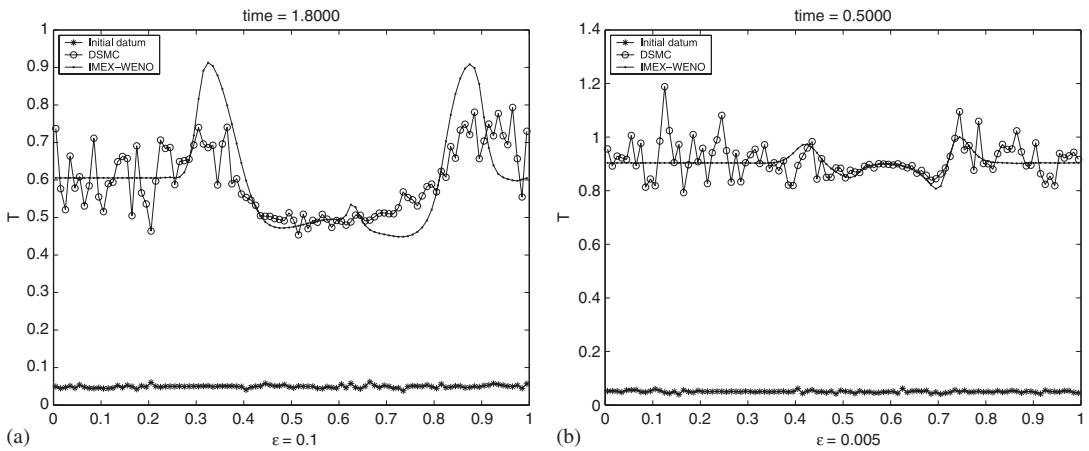

Figure 3. Test 1—evolution of the temperature with $\varepsilon = 0.1$ (a) and $\varepsilon = 0.005$ (b).

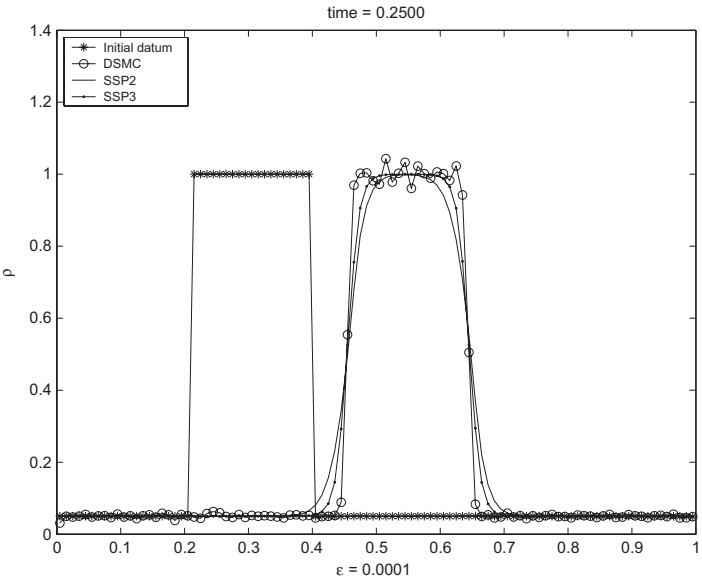

Figure 4. Test 1—evolution of the mass density with $\varepsilon = 0.0001$.

When the value of ε decreases, the equilibrium conditions $u = u_b$ and $T = T^\sharp$ are achieved faster. In particular, when $\varepsilon = 10^{-4}$ the equilibrium is reached in a few time steps and the impurities are just transported with velocity u_b and temperature $T^\sharp$. In this case (Figures 4–6) we also report the results of the third-order IMEX-SSP3(4, 3, 3) schemes which clearly shows the better resolution of the discontinuity.

DOI: 10.1002/fld

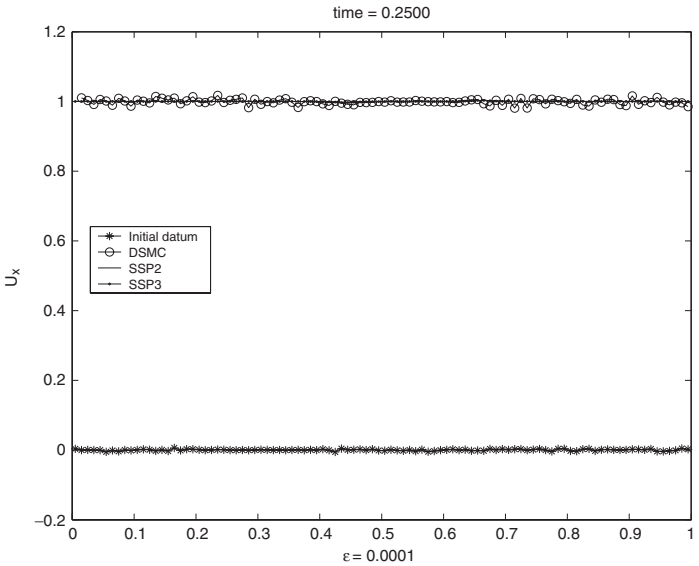

Figure 5. Test 1—evolution of the velocity with $\varepsilon = 0.0001$.

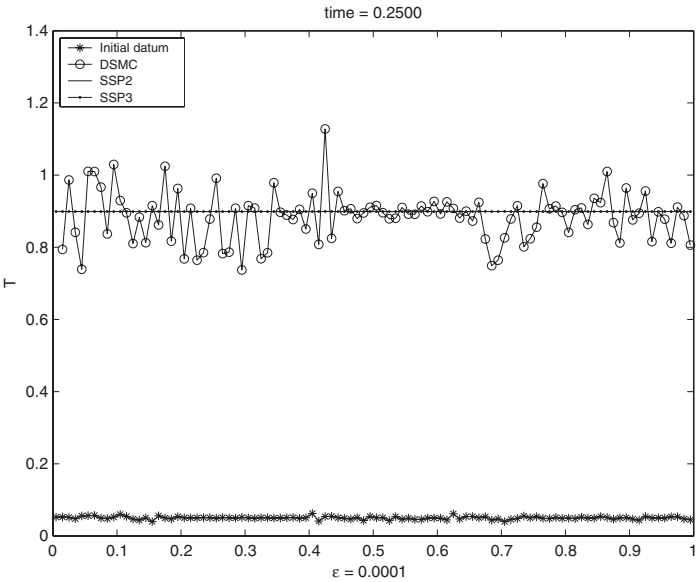

Figure 6. Test 1—evolution of the temperature with $\varepsilon = 0.0001$.

5.2. *Concentrations of impurities with different mean velocities*

In this test we consider two concentrations of impurities characterized, respectively, by $\rho = 1$ for $0.1 \leqslant x \leqslant 0.3$ and $\rho = 0.6$ for $0.5 \leqslant x \leqslant 0.7$ ($\rho = 0$ elsewhere), the first one having zero mean velocity

DOI: 10.1002/fld

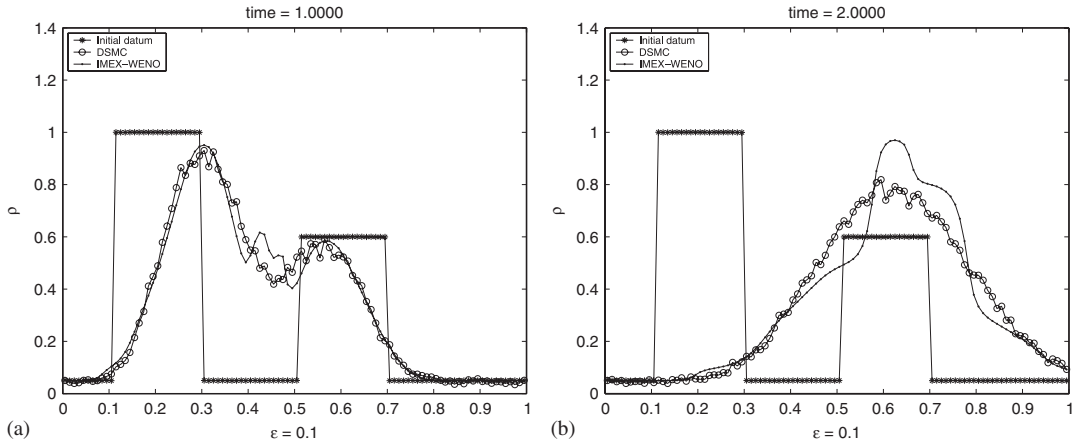

Figure 7. Test 2—evolution of the mass density with $\varepsilon = 0.1$ at $t = 1$ and 2.

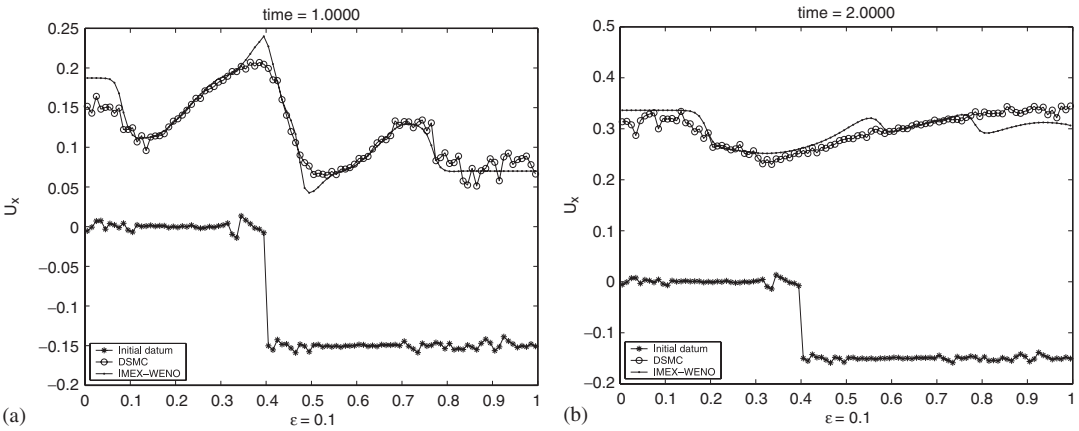

Figure 8. Test 2—evolution of the velocity with $\varepsilon = 0.1$ at $t = 1$ and 2.

and the second one having negative mean velocity. The initial condition for velocity and temperature corresponds to a shock profile, with the following left- and right-hand side values:

$$u_{\mathrm{l}} = 0, \quad T_{\mathrm{l}} = 0.2 \quad \text{and} \quad u_{\mathrm{r}} = -0.15, \quad T_{\mathrm{r}} = 0.1$$

The boundary conditions are characterized by a zero flux and the evolution is studied for

$$\varepsilon = 0.1, 0.001$$

We present in Figures 7–9 the results for $\varepsilon = 0.1$ at the instants $t = 1$ and 2, and in Figures 10–12 the results for $t = 0.2$ when $\varepsilon = 0.001$. In this last case we show the results obtained with IMEX-SSP3(4, 3, 3) instead of IMEX-SSP2(2, 2, 2). Again there is good agreement between the two numerical solutions even for large values of the relaxation rate ε.

DOI: 10.1002/fld

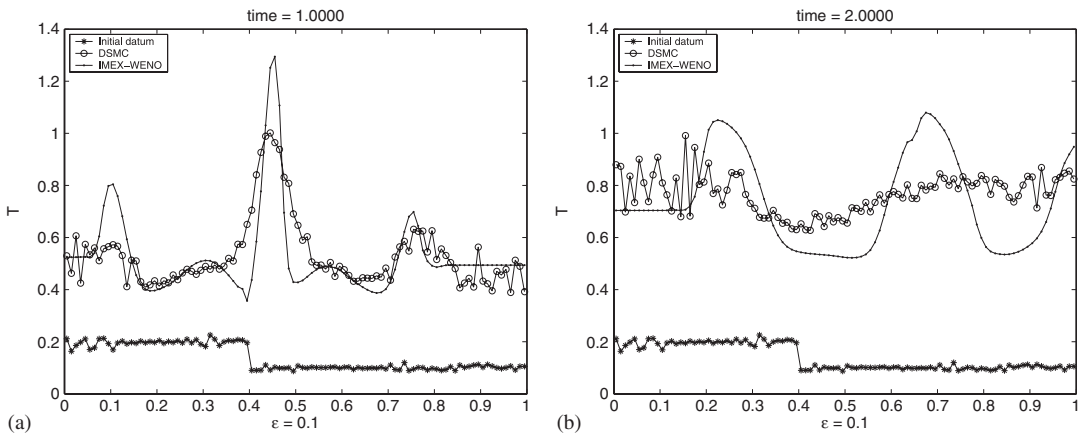

Figure 9. Test 2—evolution of the temperature with $\varepsilon = 0.1$ at $t = 1$ and 2.

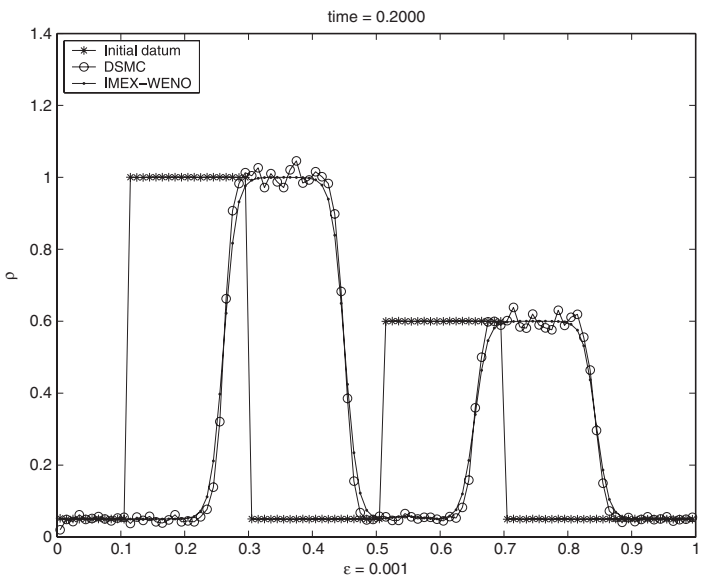

Figure 10. Test 2—evolution of the mass density with $\varepsilon = 0.001$ at $t = 0.2$.

5.3. Shock waves profiles

We finally consider a Riemann problem. In particular, we have chosen the classical Lax data

$$\rho_{\mathrm{l}} = 0.445, \quad (\rho u)_{\mathrm{l}} = 0.311, \quad E_{\mathrm{l}} = 8.928 \quad \text{and} \quad \rho_{\mathrm{r}} = 0.5, \quad (\rho u)_{\mathrm{r}} = 0, \quad E_{\mathrm{r}} = 1.4275$$

We still consider zero-flux conditions on the boundary. We present in Figures 13–18 the pictures of the solutions for the moments $\rho, \rho u, E$ at $t = 15$ and 30 for $\varepsilon = 1$ and at $t = 1$ and 2 for $\varepsilon = 0.01$. Good agreement of the two models is also observed in this case.

DOI: 10.1002/fld

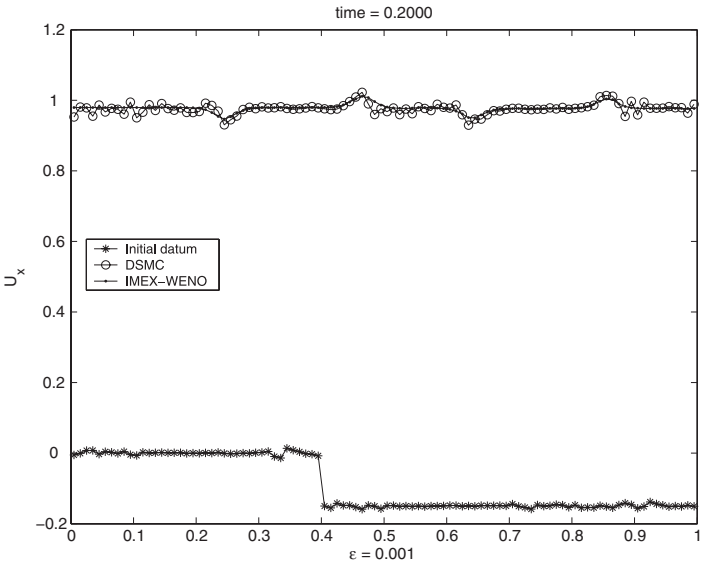

Figure 11. Test 2—evolution of the velocity with $\varepsilon = 0.001$ at $t = 0.2$.

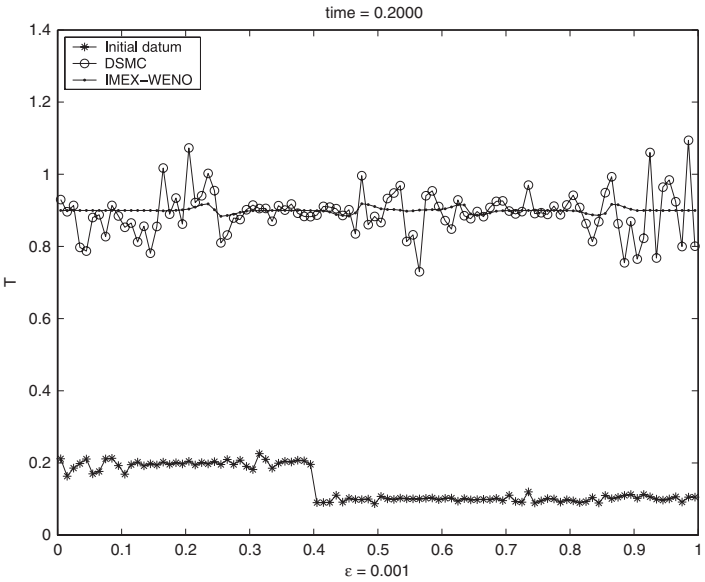

Figure 12. Test 2—evolution of the temperature with $\varepsilon = 0.001$ at $t = 0.2$.

DOI: 10.1002/fld

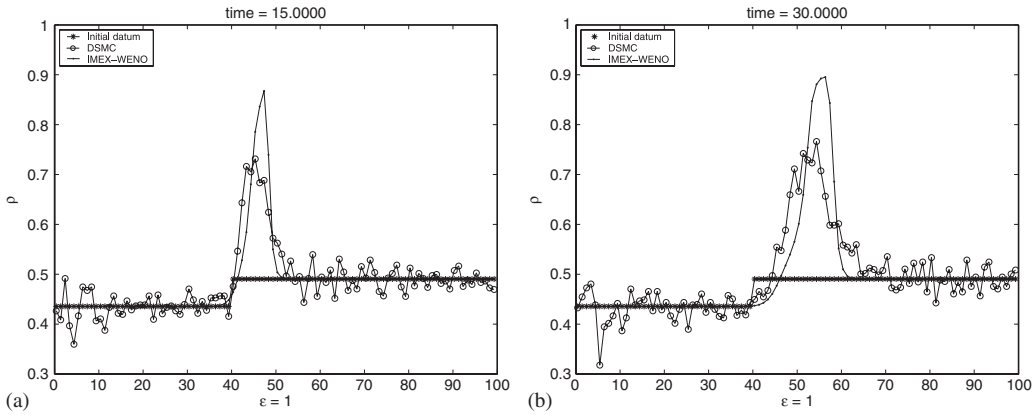

Figure 13. Test 3—evolution of the mass density with $\varepsilon = 1$ at $t = 15$ and 30.

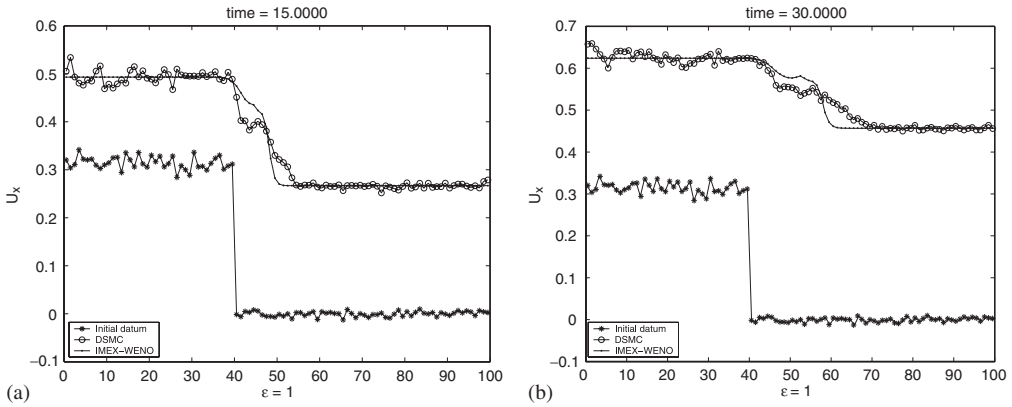

Figure 14. Test 3—evolution of the velocity with $\varepsilon = 1$ at $t = 15$ and 30.

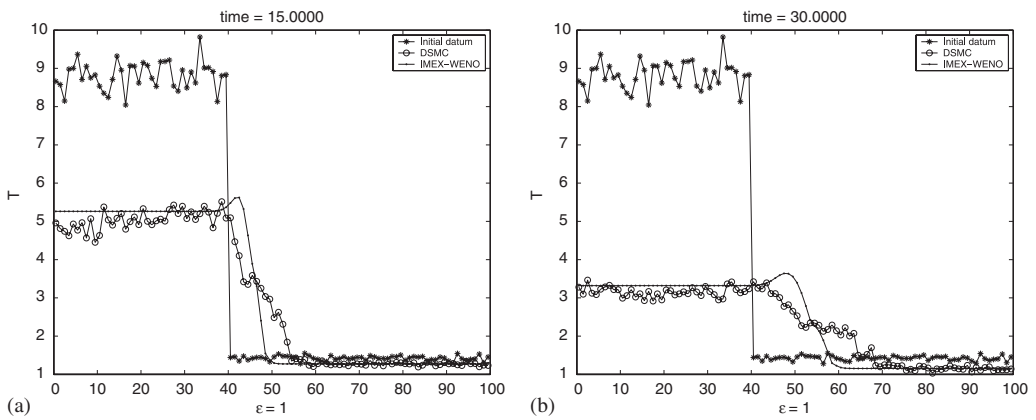

Figure 15. Test 3—evolution of the temperature with $\varepsilon = 1$ at $t = 15$ and 30.

DOI: 10.1002/fld

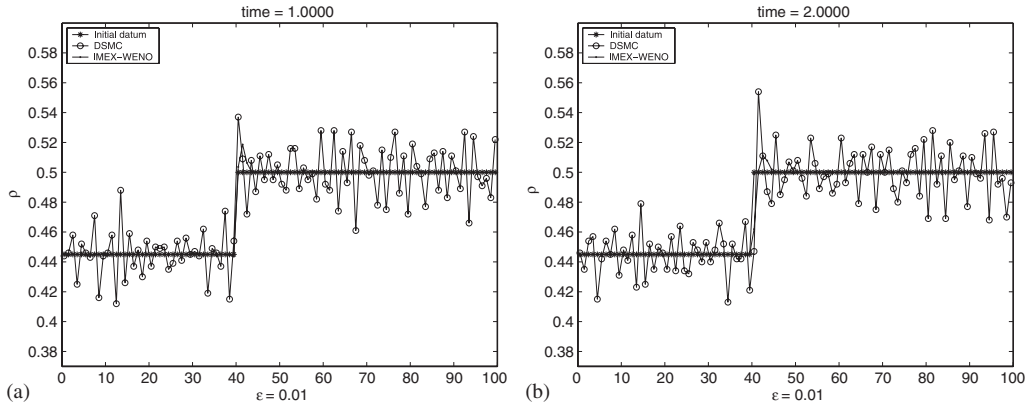

Figure 16. Test 3—evolution of the mass density with $\varepsilon = 0.01$ at $t = 1$ and 2.

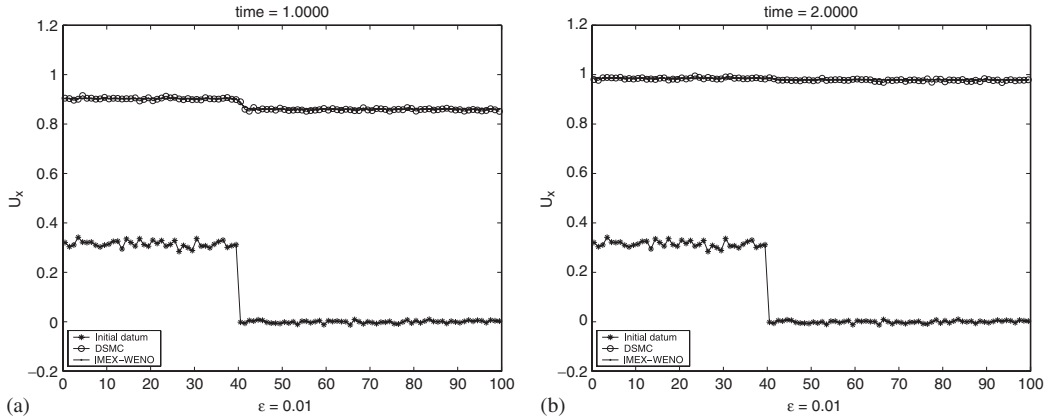

Figure 17. Test 3—evolution of the velocity with $\varepsilon = 0.01$ at $t = 1$ and 2.

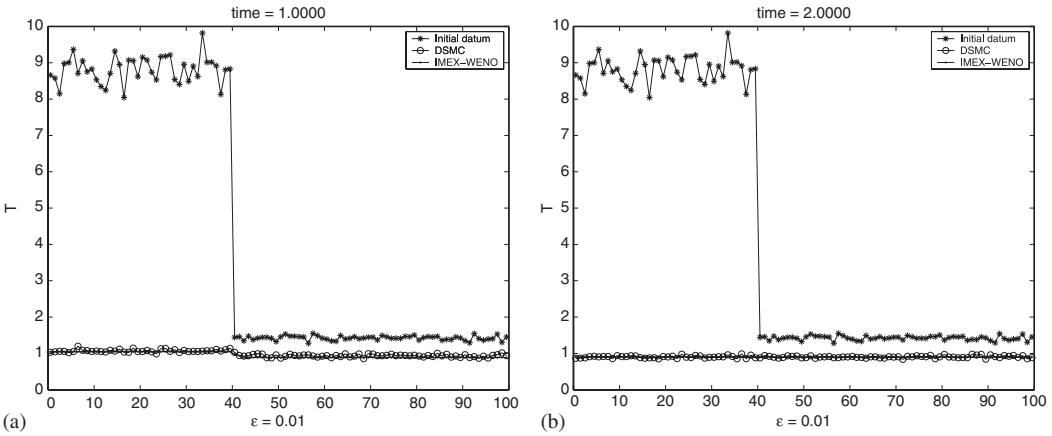

Figure 18. Test 3—evolution of the temperature with $\varepsilon = 0.01$ at $t = 1$ and 2.

DOI: 10.1002/fld

6. CONCLUSIONS

In this paper we have presented some recent results on the modelling of the diffusion of impurities in a gas. The main goal of using hydrodynamic models is the possibility to strongly reduce the computational cost of the full kinetic model. This is especially true when the mean free path of the particles is small.

We have introduced a Monte Carlo scheme that is suitable for the solution of the kinetic model and an IMEX-WENO method for the solution of the hydrodynamic one. For such a model the time step is independent of the mean free path between particles.

For the test cases considered here, the results obtained with the hydrodynamic model (13) are very close to the ones of the kinetic model. This is very promising for future application based on the fluid model.

The hydrodynamic model presented in this paper is derived using a logarithmic entropy functional. As described in [9] this is not the unique possibility. The choice of a quadratic entropy functional and the comparison of the corresponding model with the kinetic one are under investigation.

Finally, we hope to extend the schemes to models including some simple chemical reactions.

REFERENCES

1. Dufty JW, Santos A. Dynamics of a hard sphere granular impurity. *Physics Review Letters* 2006; **97**:058001-1–058001-4.
2. Lods B, Toscani G. The dissipative linear Boltzmann equation for hard spheres. *Journal of Statistical Physics* 2004; **117**(3–4):635–664.
3. Spiga G, Toscani G. The dissipative linear Boltzmann equation. *Applied Mathematics Letters* 2004; **17**(3):295–301.
4. Garzò V, Montanero JM. Diffusion of impurities in a granular gas. *Physics Review E* 2004; **69**.
5. Garzò V, Dufty JW. Homogeneous cooling state for a granular mixture. *Physics Review E* 1999; **60**.
6. Brey JJ, Dufty JW, Santos A. Kinetic models for granular flow. *Journal of Statistical Physics* 1999; **97**:281–322.
7. Brull S, Pareschi L. Dissipative hydrodynamic models for the diffusion of impurities in a gas. *Applied Mathematics Letters* 2006; **19**(6):516–521.
8. Bobylev AV, Carrillo JA, Gamba IM. On some properties of kinetic and hydrodynamic equations for inelastic interactions. *Journal of Statistical Physics* 2000; **98**:743–773.
9. Bisi M, Spiga G. Fluid-dynamic equations for granular particles in a host medium. *Journal of Mathematics Physics* 2005; **46**(113301):1–20.
10. Ferrari E, Pareschi L. Hybrid Monte Carlo methods for the diffusion of impurities in a gas. In *Modelling and Numerics of Kinetic Dissipative Systems*, Pareschi L, Russo G, Toscani G (eds). Nova-Science: New York, 2006; 191–204.
11. Pareschi L, Russo G. Time Relaxed Monte Carlo methods for the Boltzmann equation. *SIAM Journal on Scientific Computing* 2001; **3**:1253–1273.
12. Pareschi L, Trazzi S. Numerical solution of the Boltzmann equation by time relaxed Monte Carlo (TRMC) methods. *International Journal for Numerical Methods in Fluids* 2005; **48**:947–983.
13. Pullin DI. Generation of normal variates with given sample. *Journal of Statistical Computation and Simulation* 1979; **9**:303–309.
14. Pareschi L, Russo G. An introduction to Monte Carlo methods for the Boltzmann equation. *ESAIM Proceedings*, Paris, vol. 10, 1999; 35–76.
15. Pareschi L, Russo G. Implicit-explicit Runge–Kutta schemes and applications to hyperbolic systems with relaxation. *Journal of Scientific Computing* 2005; **25**(1–2):129–155.

DOI: 10.1002/fld

16. Shu C-W. Essentially non-oscillatory and weighted essentially non-oscillatory schemes for hyperbolic conservation laws. In *Advanced Numerical Approximation of Nonlinear Hyperbolic Equations*, Lecture Notes in Mathematics, vol. 1697, Springer: Berlin, 1998; 325–432.
17. Shu C-W, Osher S. Efficient implementation of essentially nonoscillatory shock-capturing schemes. *Journal of Computational Physics* 1988; **77**(2):439–471.

DOI: 10.1002/fld